OPEN

Advanced imaging tools for evaluating cardiac morphological and functional impairment in hypertensive disease

Maria Lembo, Maria Virginia Manzi, Costantino Mancusi, Carmine Morisco, Maria Assunta Elena Rao, Alberto Cuocolo, Raffaele Izzo, and Bruno Trimarco

Arterial hypertension represents a systemic burden, and it is responsible of various morphological, functional and tissue modifications affecting the heart and the cardiovascular system. Advanced imaging techniques, such as speckle tracking and three-dimensional echocardiography, cardiac magnetic resonance, computed tomography and PET-computed tomography, are able to identify cardiovascular injury at different stages of arterial hypertension, from subclinical alterations and overt organ damage to possible complications related to pressure overload, thus giving a precious contribution for guiding timely and appropriate management and therapy, in order to improve diagnostic accuracy and prevent disease progression. The present review focuses on the peculiarity of different advanced imaging tools to provide information about different and multiple morphological and functional aspects involved in hypertensive cardiovascular injury. This evaluation emphasizes the usefulness of the emerging multiimaging approach for a comprehensive overview of arterial hypertension induced cardiovascular damage.

Keywords: 3D-echocardiography, arterial hypertension, cardiac magnetic resonance, computed tomography, speckle tracking echocardiography

Abbreviations: AH, arterial hypertension; ^{18}F-FDG, fluorine-18-fluorodeoxyglycose; ^{18}F-NaF, fluorine-18-sodium fluoride; 2D, two-dimensional; 3D, three-dimensional; CT, computed tomography; ECV, extracellular volume fraction; EDV, end-diastolic volume; GLS, global longitudinal strain; LGE, late gadolinium enhancement; LVH, left ventricular hypertrophy; LVM, left ventricular mass; PET-CT, PET-computed tomography

INTRODUCTION

Arterial hypertension (AH) represents a relevant cardiovascular risk factor and a systemic burden [1,2]. It has, in fact, an important impact on the development of cardiac and vascular events, predisposing to heart failure, acute coronary syndromes, peripheral artery disease and stroke [3,4]. AH affects the entire body, thus leading to target organ damage in multiple districts [5].

Early diagnosis of cardiac modifications induced by pressure overload and arterial disease induced by increased arterial stiffness, together with the identification of subclinical organ damage have become crucial for a timely and adequate treatment, aiming at not only the avoidance of irreparable organ damage but also trying to confine injury progression [6].

Beyond standard echo-Doppler echocardiography, which remains among the most simple but accurate methods for the investigation of cardiac and vascular remodelling and diastolic dysfunction [1,6,7], advanced imaging techniques are emerging for their sensitive capability of recognizing early myocardial and vascular impairment in many cardiovascular diseases [8–10], including AH [11,12]. Those imaging methods, including speckle tracking and three-dimensional (3D) echocardiography, cardiac MRI, computed tomography (CT) and PET-computed tomography (PET-CT), can help, in different ways, in the detection of subclinical disease and/or in the identification of cardiovascular changes deriving from pressure overload [13–15].

The current review aims at highlighting the usefulness of advanced imaging tools, each with its peculiarity, beyond standard echocardiography, for the identification of subclinical AH-induced organ damage, revealing both myocardial morphological and functional alterations present in the hypertensive setting, even at very early stages.

TWO-DIMENSIONAL SPECKLE TRACKING ECHOCARDIOGRAPHY

Two-dimensional (2D) speckle tracking echocardiography is a feasible ultrasound tool, providing information about left ventricular deformation in different directions: longitudinal, circumferential and radial and left ventricular twisting. It was demonstrated that all speckle-tracking-derived

Journal of Hypertension 2022, 40:4–14

Department of Advanced Biomedical Sciences, Federico II University of Naples, Naples, Italy

Correspondence to Maria Lembo, MD, Department of Advanced Biomedical Sciences, Federico II University Hospital, Naples, 80100, Italy. E-mail: maria.lembo@unina.it

Received 15 June 2021 **Revised** 29 June 2021 **Accepted** 30 June 2021

DOI:10.1097/HJH.0000000000002967

strains appeared to be altered in patients affected by AH [16]. In particular, global longitudinal strain (GLS), despite being load dependent, is a sensitive parameter for identification of left ventricular subclinical systolic dysfunction, and it is related to the amount of myocardial fibrosis and left ventricular filling pressures [17,18]. In fact, it resulted impaired even in patients at very early stages of AH, independently on alterations in left ventricular geometry and before a reduction in left ventricular ejection fraction, the main used parameter for the evaluation of left ventricular systolic function, also presenting a higher reproducibility and lower interobserver and intraobserver variability than the latter [19,20].

Regional strain provided further information: longitudinal strain impairment mainly involved basal and middle segments, with a relative sparing of apical ones and resulting in higher values of relative regional strain ratio (the ratio between apical and the sum of basal and middle strain) in newly diagnosed hypertensive patients in comparison to controls, thus exacerbating the base-to-apex gradient deformation [21]. This phenomenon found correspondence in myocardial fibrosis by late gadolinium enhancement cardiac magnetic resonance, which is mainly found in left ventricular basal and middle segments in hypertensive patients with concentric left ventricular hypertrophy (LVH) [22].

Left ventricular longitudinal strain resulted progressively more impaired in hypertensive patients presenting left ventricular concentric remodelling, LVH and LVH associated with dilation. Circumferential and radial strains resulted instead compromised in more advanced stages of AH when LVH was already established, being still normal or actually increased as for radial strain and left ventricular torsion in early phases of AH, probably as a compensatory mechanism in response to pressure overload [16,23,24].

Subsequent studies showed the involvement of all the three endo, mid and subepicardial layers of both longitudinal and circumferential strains in AH [25]. At early stages of AH, longitudinal endomyocardial layer seemed to be the most affected by pressure overload [26]. Left ventricular longitudinal and circumferential endocardial and mid-myocardial layer strains progressively decreased from normotensive individuals, across patients with masked AH to patients with sustained AH [27]. Subepicardial layer strain seems to be involved in more advanced stages of AH and it was described as a prognosticator of cardiovascular events [28]. The interrelation and concomitant dysfunction of multiple strains together with the impairment of echo parameters examining different myocardial layers (e.g. the independent association between GLS, quantifying the deformation of longitudinal fibres and midwall fractional shortening evaluating the motion of midwall circumferential fibres), demonstrated the comprehensive left ventricular systolic dysfunctional dynamics in AH [16,29]. Furthermore, longitudinal and circumferential early diastolic strain rates were decreased, while late diastolic strain rates were increased in hypertensive patients, reflecting an impaired left ventricular myocardial relaxation and diastolic dysfunction [27].

In addition, investigating myocardial work components by left ventricular pressure-strain loops derived from speckle tracking echocardiography and GLS, a positive and significant correlation was found between systolic blood pressure and both global work index, representing the total work within the left ventricular pressure-strain area, and global constructive work, indicating the work performed during systolic shortening in addition to negative work during lengthening in isovolumetric relaxation, in a population of heathy individuals [30]. Those correlations were also confirmed in the hypertensive setting, where higher values of global work index and global constructive work values were highlighted in comparison to controls, in particular in patients with eccentric and concentric LVH [31]. Wasted work, which represents the work performed during segmental shortening when the aortic valve is closed in isovolumic relaxation or the work performed during systolic segmental lengthening, was also demonstrated to be higher in hypertensive patients. In addition, global efficiency, which is computed as the ratio between constructive work and wasted work of all left ventricular segments, was demonstrated to be preserved in early stages of hypertension, as higher wasted work is balanced by a higher constructive work, whereas this balance is lost in advanced stage when left ventricular dilation is established [32,33]. In addition, myocardial work index and constructive work were significantly increased in patients with uncontrolled and resistant AH in comparison to well controlled hypertensive patients and normotensive individuals. Myocardial work index was also associated with functional capacity alteration in terms of oxygen consumption [34]. In hypertensive patients, work index was positively correlated with SBP and segmental differences in work index were demonstrated, affecting especially basal segments and in particular basal septum in patients with LVH, emphasizing again the base-to-apex gradient [35].

Moreover, GLS was demonstrated to be a potential good predictor of major adverse cardiovascular events in a population of asymptomatic patients affected by hypertensive heart disease, when incorporated in a risk score, also including age more than 70 years, concentric LVH and atrial fibrillation [36].

GLS stands out among other strain types not only because its impairment is detectable even at very early stages of AH, but for its high reproducibility and as it is easily performed on board the echo machine, whereas the assessment of the other strains requires additional software.

Even if a small variability among vendors is still present, usefulness and simple approach of left ventricular GLS is considered so remarkable in different pathological conditions, including AH, that it has been considered worthy to be incorporated into the standardization of the echo report [37].

Right ventricle could also be affected by AH, as both ventricles share the interventricular septum, myocardial fibres and pericardium and this could determine ventricular interdependence. Indeed, right ventricular systolic dysfunction was demonstrated to be a remarkable prognosticator of heart failure related to AH [38]. 2D strain imaging revealed right ventricular longitudinal mechanics' dysfunction in early systemic hypertension by an impairment in peak systolic strain and early diastolic strain rate [39]. Both right ventricular GLS and longitudinal deformation of right

ventricular free-wall resulted impaired in hypertensive patients, in particular in untreated and suboptimally treated patients, and longitudinal dysfunction was more evident in the subendocardial than in the mid-myocardial right ventricular wall layer [40,41].

Speckle tracking assessment found its utility also for the evaluation of left atrial compliance.

Apart from the left and right ventricle, left atrium is another cardiac chamber being frequently affected by pressure overload. Before the development of left atrial dilation, impairment in left atrial longitudinal strain was detected in patients with suboptimal blood pressure control and AH, independently on left ventricular longitudinal dysfunction [42–44]. Left atrial peak longitudinal strain, measured at the end of the reservoir phase and left atrial peak contraction strain during left atrial systole, resulted altered even before LVH. Left atrial longitudinal strain was considered a surrogate of left ventricular diastolic dysfunction, being significantly correlated with E/e' ratio and increased left ventricular filling pressures [45,46].

Moreover, in hypertensive patients with concomitant paroxysmal atrial fibrillation, speckle tracking-derived left atrial reservoir, conduit and pump function were all early impaired [47].

Even if not as widely validated as for left ventricular and left atrial assessment, speckle tracking echo was also applied on vascular districts [48]. In particular, circumferential strain analysed in common carotid arteries was demonstrated to be significantly correlated with carotid intimalmedia thickness and arterial stiffness in a population including patients with several cardiovascular risk factors and a high prevalence of AH [49].

Table 1 summarizes the information derived from advanced cardiac imaging techniques for detection of left ventricle (LV), left atrial and vascular damage, according to the possibility to identify morphological and functional abnormalities at an early stage, consolidated stage of AH or possibly diagnosing AH complications (Fig. 1).

THREE-DIMENSIONAL ECHOCARDIOGRAPHY AND THREE-DIMENSIONAL SPECKLE TRACKING ECHOCARDIOGRAPHY

Real-time 3D echocardiography allows the assessment of left ventricular geometry and in particular the computation of left ventricular mass (LVM) and left ventricular end-diastolic volume (EDV) and end-systolic volume, providing an accuracy that is comparable to MRI, the latter considered the gold standard for this evaluation [50–52]. 3D-echocardiographic technique could represent a good compromise between two-dimensional echocardiography and MRI: it shows indeed advantages over standard 2D-echo, as it does not need geometrical assumptions and could overcome some limitations due to off-axis beam orientation and difficult evaluation of asymmetric LVH; it is also less expensive than MRI [53].

Recently, the use of LVM/EDV ratio, the so-called left ventricular remodelling index, already validated by MRI, has been proposed for the 3D-echocardiographic evaluation of left ventricular geometry in the hypertensive setting [54]. Higher values of LVM/EDV ratio correspond to the increase of left ventricular wall thickness in relation with left ventricular internal cavity size. Elevated values of LVM/EDV ratio by MRI were associated with more extended areas of left ventricular myocardial fibrosis and with poor prognosis in hypertensive patients [13,55]. In a population of newly diagnosed and never-treated hypertensive patients, the use of LVM/EDV ratio by 3D-echo was able to recognize a higher rate of hypertensive patients with left ventricular concentric remodelling in comparison to 2D-derived relative wall thickness; these patients also presented an impairment in both systolic dynamics, with GLS and stroke volume reduction, and diastolic function, with higher values of E/e' ratio [15,54]. Hypertensive women, being more likely to develop left ventricular concentric remodelling in response to pressure overload, presented higher values of 3D-LVM/EDV ratio than men [54,56].

3D-speckle tracking derived strains provide further information. The use of 3D-speckle tracking examination has the advantage over 2D assessment of allowing the evaluation of the entire LV from a single volume of data acquired from the apical probe position, without the need of multiple views acquisition, thus substantially reducing time of acquisition and analysis. From this technique, information about GLS, global circumferential and global radial strain, left ventricular twisting and torsion are obtainable, similarly to 2D-strain evaluation [57]. In addition to these strains, 3D-speckle tracking produces info about a further strain: global area strain, which is the percentage change of the myocardium from its original dimensions, thus a combination of both longitudinal and circumferential deformation. An impairment of all those strains, including global area strain, was observed in hypertensive patients, even in very young patients and in ones at early stages of AH [57,58]. In addition, the progression towards left ventricular geometrical remodelling induced by pressure overload exacerbated left ventricular deformation impairment, strains being more reduced, in absolute value, in hypertensive patients with concomitant LVH and dilation, according to different left ventricular geometrical patterns [16,59]. The main limitation to the use of 3D-echocardiographic approach is the vendor dependent variability and the suboptimal feasibility, which is a little lower than the standard 2D-echo approach [60]. However, improvements and advancements in transducers' technology allow, nowadays, the acquisition of the volume data set in a single heartbeat, thus overcoming some feasibility issues due to arrhythmias or incapability in breath holding.

3D-echo found application even for the evaluation of right ventricular volumes and ejection fraction. At consolidated stages of AH, 3D RV end-systolic volume and EDV were increased, while right ventricular ejection fraction resulted reduced in patients with any type of LVH; this feature was indeed particularly evident in hypertensive patients presenting left ventricular dilation associated with LVH [61].

3D-approach was also recently used to identify early left atrial morphological and functional alterations. In particular, left atrial phasic volumes were found to correlate with

TABLE 1. Advanced cardiac imaging techniques for detection of left ventricular, left atrial and vascular damage induced by arterial hypertension

Left ventricle			
Tool	**Early stage**	**Consolidated stage**	**Complications**
2D speckle tracking echo	GLS impairment Predominant basal and middle LS involvement Layers' function impairment, especially longitudinal endomyocardial layer. Myocardial work: higher global work index and global constructive work	GLS, circumferential and radial strains impairment more evident with LV hypertrophy Layers' function impairment Myocardial work: higher global work index and global constructive work, higher wasted work	
3D echocardiography and 3D speckle tracking	Increased LVM/EDV ratio Concentric remodelling with reduced stroke volume All strains impairment: including GLS, global circumferential, radial and area strain.	LV hypertrophy	LV dilation and heart failure
MRI	Impaired LV strains by feature tracking LV diastolic dysfunction	LV hypertrophy Basal and middle segments LGE, with no ischemic pattern LV diffuse and local fibrosis: elevated ECV and native T1 Impaired LV strains by feature tracking LV diastolic dysfunction	LV dilation and heart failure
CT	LV diastolic dysfunction	LV hypertrophy Diffuse fibrosis by CT ECV LV diastolic dysfunction	Coronary artery disease Aortic valve stenosis and Agaston calcium score
PET-CT		Increased LV ^{18}F-FDG uptake, with higher inflammation	Increased LV ^{18}F-NaF uptake and ^{18}F-FDG in aortic valve stenosis Increased LV ^{18}F-NaF uptake and ^{18}F-FDG in coronary atherosclerosis Rubidium-82 reduced myocardial perfusion reserve
Right ventricle			
Tool	**Early stage**	**Consolidated stage**	**Complications**
2D speckle tracking echo	Impaired RV GLS and free-wall LS	Impaired RV GLS and free-wall LS. Layers' function impairment, especially longitudinal endomyocardial layer	
3D echocardiography and 3D speckle tracking		3D RV volumes were increased and 3D RV ejection fraction resulted reduced in patients with LV hypertrophy	
MRI		Increased RV mass index, ventricular wall thickness and remodelling index	
Left atrium			
Tool	**Early stage**	**Consolidated stage**	**Complications**
2D speckle tracking echo	LA strain impairment: reduced LA reservoir, conduit and pump function		
3D echocardiography and 3D speckle tracking	LA strain impairment	LA strain impairment and dilation	
MRI	LA strain impairment by feature tracking	LV strain impairment and dilation	
CT		LV dilation	
Vessels			
Tool	**Early stage**	**Consolidated stage**	**Complications**
2D speckle tracking echo	Impaired circumferential vascular strain in carotids		
MRI			Aortic aneurism Carotid plaques
CT			Coronary artery disease Carotid plaques Aortic aneurism Acute aortic syndromes Stroke
PET-CT			Increased ^{18}F-FDG uptake in carotid atheroma Increased LV ^{18}F-NaF uptake in coronary atherosclerosis and carotid plaques

18F-FDG, fluorine-18-fluorodeoxyglycose; 18F-NaF, fluorine-18-sodium fluoride; 2D, two-dimensional; 3D, three-dimensional; CT, computed tomography; ECV, extracellular volume fraction; GLS, global longitudinal strain; LA, left atrial; LS, longitudinal strain; LV, left ventricular; LVM/EDV ratio, left ventricular mass/end-diastolic volume ratio; PET-CT, PET-computed tomography.

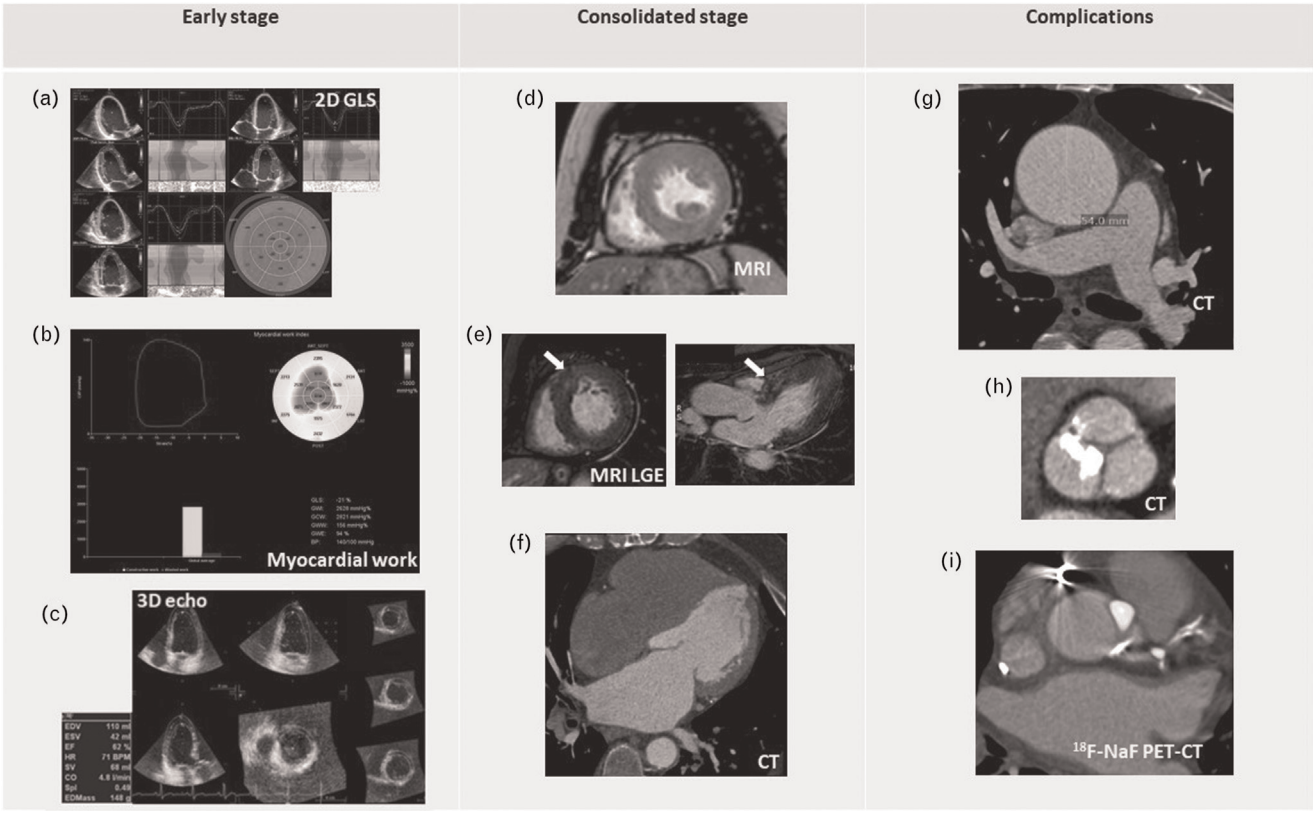

FIGURE 1 Example showing alterations provided by different advanced imaging tools at early stage, consolidated stage of arterial hypertension and complications. At early stages: (a) 2D GLS and regional strain impairment with predominant involvement of basal and middle longitudinal strain, (b) Myocardial work components alteration in hypertensive patients, (c) LV concentric geometry with increased LVM/EDV ratio detectable at 3D-echocardiography. At consolidated stage: (d) LVH evaluated by MRI, E) LGE nonischemic intramyocardial pattern (white arrow) of the basal anterior septum (left: basal short axis view, right: three-chamber view) in a hypertensive patient with LVH, (f) contrast-enhanced CT showing LA dilation. Complications: (g) Aneurism of the ascending aorta detected by contrast-CT, (h) Aortic valve calcification and stenosis by CT, (i) ^{18}F-NaF PET-CT showing uptake within both the descending left coronary artery and the aortic valve. ^{18}F-NaF, fluorine-18-sodium fluoride; 2D, two-dimensional; 3D, three-dimensional; CT, computed tomography; EDV, end-diastolic volume; GLS, global longitudinal strain; LA, left atrial; LV, left ventricular; LVH, left ventricular hypertrophy; LVM, left ventricular mass; PET-CT, PET-computed tomography.

organ damage induced by AH and 3D-speckle tracking derived left atrial strains resulted early altered in hypertensive patients, even before left atrial dilation [62,63]. Higher cumulative SBP from early adulthood throughout middle age was associated with adverse left atrial remodelling, with higher left atrial volumes, increased reservoir, and impaired early diastolic strain rate indicating impaired conduit function. Thus, pressure overload has an early and cumulative impact on both left atrial structure and function. Alteration of 3D LA dynamics and volumes reflect the severity and chronicity of left ventricular diastolic dysfunction, being correlated to left ventricular filling pressures [64].

MRI

Cardiac MRI supplies multiple valuable information not only about left ventricular geometry and function, but also providing tissue characterization. Indeed, MRI is considered the gold standard for the assessment and evaluation of left ventricular mass and volumes, thanks to the optimal spatial resolution and tracing of epicardial and endocardial borders [65]. MRI allows to identify different pathological left ventricular geometrical patterns possibly present in AH: left ventricular concentric remodelling, eccentric and concentric LVH associated or not with left ventricular dilation [66]; left ventricular dilation being related with the highest risk of mortality [67]. In addition, MRI is extremely useful for guiding differential diagnosis of LVH: the possibility to combine information deriving from left ventricular geometry (thus also detect asymmetrical segmental hypertrophy) with tissue characterization and derived myocardial fibrosis' extension and localization allows the discrimination between LVH linked to hypertensive hearts and other pathological conditions, such as infiltrative and storage cardiomyopathies, hypertrophic cardiomyopathy, athlete's heart [22,68,69]. Areas of myocardial replacement fibrosis are characterized by increased extracellular volume distribution, causing delayed gadolinium wash-out and thus detection of regions of late gadolinium enhancement (LGE). In AH-induced LVH, the presence of noninfarcted LGE patterns were recognised in about 50% of the patients, most frequently involving basal and middle segments [22]. It was also demonstrated that there was a significant correlation between the extension of LGE and the degree of left ventricular diastolic dysfunction [70]. On the contrary, in AH patients, a diffuse myocardial fibrosis is often present, which is not detectable by LGE. Indeed, T1 mapping and the evaluation of extracellular volume fraction (ECV) were

introduced with this aim. T1, expressing tissues' longitudinal relaxation time, is evaluated before and after gadolinium administration: native T1 values reflect the composite signal of both myocardial cells and interstitium, while postcontrast values give information about extracellular space. The computation of ECV is derived from a formula including pre and postcontrast T1 values of the myocardium and blood pool together with haematocrit [71,72]. In the hypertensive setting, several studies demonstrated high values of ECV and native T1 in AH patients, both being associated with left ventricular mass and LVH [73–75]. In fact, examining different patterns of left ventricular geometry related to AH, patients with LVH had significantly higher values of ECV and native T1 in comparison to those with normal left ventricular mass, whose values were comparable to those of healthy controls [13,75]. In addition, elevated ECV identified by T1 mapping in hypertensive hearts resulted associated with multiple inflammation biomarkers [75].

As AH represents a well known risk factor for the development of coronary artery disease involving both epicardial coronary arteries and coronary microcirculation, stress cardiac MRI assessment with adenosine or dipyridamole can evaluate the presence of inducible ischemia. Stress MRI by first pass gadolinium during a vasodilator stressor injection can differentiate patients with small vessel disease from those with epicardial coronary stenosis, evaluating the temporal and spatial extent of the perfusion deficits. On the contrary, subendocardial LGE can also permit to localize and quantify zones of myocardial necrosis following myocardial infarction [76,77].

Morphological and functional right ventricular adaptation to systemic pressure overload mostly reflects the modifications affecting the LV. In hypertensive patients, significant positive biventricular correlations were demonstrated between indexed mass, early peak filling rate and ejection fraction by MRI. Right ventricular mass index, ventricular wall thickness and remodelling index measured by MRI were higher in hypertensive patients than in controls [78].

Similarly to CT, MRI can provide information about morphological changes of heart (e.g. left atrial dilation) and of the cardiovascular district, thus including the possibility to uncover abnormal aortic dilation, possibly related to AH, at different districts: aortic root, arch, thoracic or abdominal aorta [79], with the advantage of not using ionizing radiation and potentially high nephrotoxic contrast agents. Furthermore, MRI is a valuable method for the evaluation of carotid plaques, both for the estimation of lumen stenosis and for the assessment of plaques' composition, also allowing detection of lipid-rich necrotic core and intraplaque haemorrhage [80]. In the hypertensive setting, the identification of those vulnerable plaques could predict the risk of cerebrovascular events [81].

Even with MRI, it is possible to investigate myocardial deformation and strains likewise speckle tracking for echocardiography. Feature-tracking, which is an optical flow method, able to detect feature in images and track them during the cardiac cycle, allows the evaluation of GLS, global circumferential and radial strains. It is a postprocessing method and one of the most recent used, having the advantage over myocardial deformations methods, such as cardiac tagging or displacement encoding with stimulated echoes, to not need additional images acquisition [82,83]. Similarly to speckle tracking echo, feature-tracking derived strains were all demonstrated to be altered in patients affected by AH, strains being more impaired in patients with LVH [84]. In patients with hypertensive heart disease MRI-derived strains were related to both left ventricular mass and ECV [85]. The negative association between GLS by feature tracking and concentric geometry evaluated by LVM/EDV ratio was also confirmed by MRI, similarly to 3D-echocardiography [86].

Feature-tracking has been used also for the investigation of left atrial function; in AH, left atrial reservoir and conduit dysfunction were early identified in patients, even before the development of LVH [87]. These parameters correlated with E/A ratio, thus with left ventricular diastolic dysfunction. Apart from left ventricular and left atrial strain imaging, info about left ventricular diastolic function can be obtained by MRI, even if standard Doppler echo is the first level and more simple way to assess it. Left atrial enlargement, using biplane area-length method, suggests elevated left ventricular filling pressure and chronic diastolic dysfunction. Similarly to echo-Doppler assessment, phase-contrast MRI allows the evaluation of transmitral flow with E and A velocities, by placing a reference plane perpendicular to mitral inflow at the mitral valve leaflet tips. In addition, the pulmonary vein flow can be measured 1 cm into the pulmonary vein ostium. In hypertensive patients a strong relationship between MRI-derived and Doppler-derived velocities was demonstrated and MRI-derived diastolic dysfunction well correlated with left ventricular invasively measured filling pressures [88]. With technological advancement, the quantification of flow was also possible with 3D spatial encoding and four-dimensional phase contrast-MRI [89].

COMPUTED TOMOGRAPHY

ECG-gated contrast-enhanced CT is very useful for anatomical assessment. In AH, for what concern the myocardium, CT evaluation of LVH and left atrial dilation can be performed, even if echocardiography or MRI are preferred for this analysis because free of ionizing radiations [90]. Diastolic dysfunction can be also assessed by dual-source CT with the evaluation of left atrial phasic volumes and function parameters. In addition, transmitral peak velocity could be calculated by dividing peak diastolic transmitral flow by the corresponding mitral valve area and mitral septal tissue velocity computed from changes in left ventricular length per cardiac phase for the estimation of left ventricular filling pressures. These diastolic measures presented good correlation with echo assessment [91].

Similarly to MRI, diffuse myocardial fibrosis can be detected by ECV applied to CT or dual energy CT. ECV computation again is based on haematocrit and pre and postcontrast Hounsfield unit attenuation in the myocardium and blood pool. This technique was tested in a population also including hypertensive patients, with a very good correlation between ECV by CT and ECV by MRI [92]. Thus, the possibility to noninvasively analyse myocardial fibrosis

by CT, even if needing validation on wider population cohorts, has the advantage to be assessed in patients for whom MRI is precluded because of claustrophobia or non-MRI compatible implants [93].

CT has an important role in the identification and evaluation of complications related to AH. The high spatial resolution makes CT the chosen imaging method for vessels analysis. AH is associated with arterial stiffness and high mechanical stress on the aortic wall, thus resulting in alteration of aortic elastic properties and dilatation, possibly involving both thoracic and abdominal aorta [94]. The dilation of abdominal aorta has prognostic implications since it was demonstrated to be related to long-term mortality [95]. CT is, in fact, used for surveillance and for guiding surgical timing and management in patients experiencing a thoracic or abdominal aortic aneurysm, not only providing optimal views for the determination of aneurysm size and extension, but also for diagnosis of acute aortic syndromes including aortic dissections and intramural aortic hematoma, also possible complications related to AH [96,97]. In addition, AH is also one of the main risk factors for the development of coronary artery disease, as it induces endothelial coronary damage and accelerates atherosclerosis and plaque generation, and ECG-gated contrast CT provides the estimation of coronary stenosis and lumen patency [98]. CT can be also assessed to obtain information about carotid plaques composition and in particular for the evaluation of calcific volume, demonstrated to be largely present in hypertensive patients [80,99].

CT is also a valuable technique for the analysis of aortic valve. Aortic stenosis and AH often coexist, as increased pressure overload could determine a mechanical stress on the aortic leaflets, with consequent endothelial damage and development of valve stenosis [100,101]. CT could be extremely helpful in aortic stenosis grading with the possibility to evaluate calcification degree by Agaston calcium score on noncontrast CT scans, particularly in those patients in whom the echocardiographic examination is suboptimal and there is a mismatch between different echocardiographic parameters for aortic stenosis estimation [102]. In this regard, paradoxical low flow low gradient aortic stenosis is a particular type of aortic valve stenosis, characterized by a discrepancy between echocardiographic mean pressure gradient and aortic valve area, often difficult to distinguish from pseudo-severe aortic stenosis by the echocardiographic evaluation alone; it was described in hypertensive hearts with left ventricular concentric geometry and small diameters and associated with unfavourable prognosis [103].

PET-COMPUTED TOMOGRAPHY

Molecular imaging with PET-CT is emerging for its ability in detection subclinical disease in multiple settings [104–106].

Different tracers provide information about different pathological mechanisms developed in diseases, including AH. Fluorine-18-fluorodeoxyglycose (^{18}F-FDG) is a glucose analogous; an increased uptake of this tracer reflects cell active metabolism and proliferation, and it is associated with inflammation [104]. Left ventricular myocardial ^{18}F-FDG uptake was demonstrated to be higher in patients affected by AH, it being positively correlated to both systolic and diastolic blood pressure values [107]. In addition, AH enhances the development of arterial atherosclerosis and related inflammation [108]. ^{18}F-FDG is able to detect and quantify the arterial inflammatory processes in atherosclerotic plaques [109,110]. In particular, ^{18}F-FDG uptake in carotid atheroma resulted associated with a high risk of recurrent cerebrovascular events [111].

On the other hand, fluorine-18-sodium fluoride (^{18}F-NaF) is able to evaluate microcalcification activity, exchanging with hydroxyl groups on exposed regions of hydroxyapatite crystals on calcification surface [112,113]. Thus, it is extremely useful to study calcification remodelling in atherosclerotic plaques and valve diseases, both possibly related to AH condition. It was demonstrated that both diastolic and mean blood pressure values were independently associated with the extent of coronary atherosclerosis as quantified by ^{18}F-NaF [114]. In addition, in a population including a high percentage of hypertensive patients, carotid 18F-NaF uptake was associated with severity of ischemic cerebrovascular disease [115]. For what concerns aortic valve stenosis, both ^{18}F-FDG and ^{18}F-NaF uptake resulted increased in patients with aortic stenosis. Moreover, ^{18}F-NaF activity showed to be progressively increased in patients with higher disease severity [116].

Rubidium-82 PET-CT allows the evaluation of myocardial perfusion reserve, characterizing the capability of vasodilation of the coronary circulation. Hypertensive patients, in particular those with resistant hypertension, were demonstrated to exhibit lower values of myocardial perfusion reserve and this parameter was related with a higher rate of cardiovascular events, demonstrating both coronary and microvascular dysfunction and the prognostic value of myocardial perfusion reserve in this setting [117].

Even if needing wider studies on hypertensive population settings, PET-CT assessments with different tracers provide promising basis for studying molecular imaging and provide possibly prognosticators of disease progression.

CONCLUSION

The great advancements in imaging techniques allow the evaluation of AH condition and influence on the myocardium and the cardiovascular system from multiple points of view, from tools bringing to light subclinical dysfunction as speckle tracking echocardiography, to instruments allowing evaluation of tissue characterization and possible AH complication as MRI and CT, and molecular imaging highlighting active metabolism, calcification activity or microvascular dysfunction. Different imaging tools are able to detect morphological and functional abnormalities related to AH, but, on the contrary, every single technique owns its peculiarity and provides complementary information (Fig. 2).

A multiimaging approach thus may help to have a more exhaustive perspective of AH-induced damage, thus contributing to assess an early diagnosis, avoid disease progression and provide appropriate treatments for patients' optimal management.

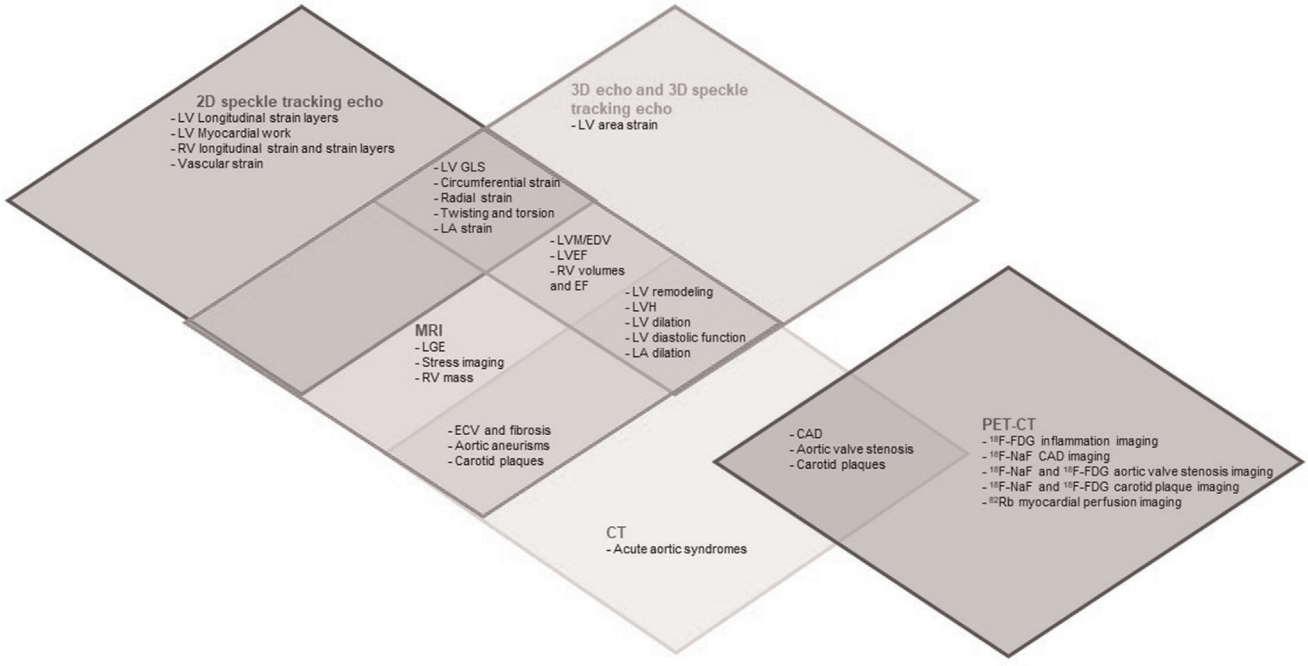

FIGURE 2 Schema depicting the advanced imaging tools useful in the cardiac and vascular damage induced by arterial hypertension; some evaluations are common to one or more techniques while each method owns its peculiarities. ^{18}F-FDG, fluorine-18-fluorodeoxyglycose; ^{18}F-NaF, fluorine-18-sodium fluoride; 2D, two-dimensional; 3D, three-dimensional; CAD, coronary artery disease; CT, computed tomography; ECV, extracellular volume fraction; EDV, end-diastolic volume; GLS, global longitudinal strain; LA, left atrial; LGE, late gadolinium enhancement; LV, left ventricular; LVH, left ventricular hypertrophy; LVM, left ventricular mass; PET-CT, PET-computed tomography.

ACKNOWLEDGEMENTS

M.L. is part of the PhD program in Cardiovascular Pathophysiology and Therapeutics (CardioPaTh).

Conflicts of interest

There are no conflicts of interest.

REFERENCES

1. Williams B, Mancia G, Spiering W, Agabiti Rosei E, Azizi M, Burnier M, *et al.* ESC/ESH Guidelines for the management of arterial hypertension. *J Hypertens* 2018; 36:1953–2041.
2. Chow CK, Teo KK, Rangarajan S, Islam S, Gupta R, Avezum A, *et al.* Prevalence, awareness, treatment, and control of hypertension in rural and urban communities in high-, middle-, and low-income countries. *JAMA* 2013; 310:959–996.
3. Rapsomaniki E, Timmis A, George J, Pujades-Rodriguez M, Shah AD, Denaxas S, *et al.* Blood pressure and incidence of twelve cardiovascular diseases: lifetime risks, healthy life-years lost, and age-specific associations in 1.25 million people. *Lancet* 2014; 383:1899–1911.
4. Kisialiou A, Grella R, Carrizzo A, Pelone G, Bartolo M, Zucchella C, *et al.* Risk factors and acute ischemic stroke subtypes. *J Neurol Sci* 2014; 339:41–46.
5. Lewington S, Clarke R, Qizilbash N, Peto R, Collins R. Age-specific relevance of usual blood pressure to vascular mortality: a meta-analysis of individual data for one million adults in 61 prospective studies. *Lancet* 2002; 360:1903–1913.
6. Cameli M, Lembo M, Sciaccaluga C, Bandera F, Ciccone MM, D'Andrea A, *et al.* Identification of cardiac organ damage in arterial hypertension: insights by echocardiography for a comprehensive assessment. *J Hypertens* 2020; 38:588–598.
7. Sorrentino R, Esposito R, Santoro C, Vaccaro A, Cocozza S, Scalamogna M, *et al.* Practical impact of new diastolic recommendations on noninvasive estimation of left ventricular diastolic function and filling pressures. *J Am Soc Echocardiogr* 2020; 33:171–181.
8. Tufano A, Di Minno MND, Guida A, Lembo M, Di Minno G, Galderisi M. Cardiac manifestations of antiphospholipid syndrome: clinical presentation, role of cardiac imaging, and treatment strategies. *Semin Thromb Hemost* 2019; 45:468–477.
9. Tufano A, Lembo M, Di Minno MN, Nardo A, Esposito R, Santoro C, *et al.* Left ventricular diastolic abnormalities other than valvular heart disease in antiphospholipid syndrome: an echocardiographic study. *Int J Cardiol* 2018; 271:366–370.
10. Cadeddu Dessalvi C, Deidda M, Mele D, Bassareo PP, Esposito R, Santoro C, *et al.* Chemotherapy-induced cardiotoxicity: new insights into mechanisms, monitoring, and prevention. *J Cardiovasc Med (Hagerstown)* 2018; 19:315–323.
11. Lembo M, Sicari R, Esposito R, Rigo F, Cortigiani L, Lo Iudice F, *et al.* Association between elevated pulse pressure and high resting coronary blood flow velocity in patients with angiographically normal epicardial coronary arteries. *J Am Heart Assoc* 2017; 6:e005710.
12. Schumann CL, Jaeger NR, Kramer CM. Recent advances in imaging of hypertensive heart disease. *Curr Hypertens Rep* 2019; 21:3.
13. Rodrigues JC, Amadu AM, Dastidar AG, Szantho GV, Lyen SM, Godsave C, *et al.* Comprehensive characterisation of hypertensive heart disease left ventricular phenotypes. *Heart* 2016; 102:1671–1679.
14. Siddiqui MA, Mittal PK, Little BP, Miller FH, Akduman EI, Ali K, Sartaj S, *et al.* Secondary hypertension and complications: diagnosis and role of imaging. *Radiographics* 2019; 39:1036–1055.
15. Lembo M, Santoro C, Sorrentino R, Trimarco B, Galderisi M, Esposito R. Impact of left ventricular mass/end-diastolic volume ratio by three-dimensional echocardiography on two-dimensional global longitudinal strain and diastolic function in native hypertensive patients. *J Hypertens* 2019; 37:2041–2047.
16. Tadic M, Cuspidi C, Majstorovic A, Kocijancic V, Celic V. The relationship between left ventricular deformation and different geometric patterns according to the updated classification: findings from the hypertensive population. *J Hypertens* 2015; 33:1954–1961.
17. Contaldi C, Imbriaco M, Alcidi G, Ponsiglione A, Santoro C, Puglia M, *et al.* Assessment of the relationships between left ventricular filling pressures and longitudinal dysfunction with myocardial fibrosis in uncomplicated hypertensive patients. *Int J Cardiol* 2016; 202:84–86.

18. Galderisi M, Trimarco B. Global longitudinal strain: a novel hallmark of cardiac risk in arterial hypertension. *J Hypertens* 2016; 34:1050–1051.
19. Lembo M, Esposito R, Lo Iudice F, Santoro C, Izzo R, De Luca N, *et al.* Impact of pulse pressure on left ventricular global longitudinal strain in normotensive and newly diagnosed, untreated hypertensive patients. *J Hypertens* 2016; 34:1201–1207.
20. Farsalinos KE, Daraban AM, Ünlü S, Thomas JD, Badano LP, Voigt JU. Head-to-head comparison of global longitudinal strain measurements among nine different vendors: the EACVI/ASE Inter-Vendor Comparison Study. *J Am Soc Echocardiogr* 2015; 28:1171–1181.
21. Lembo M, Santoro C, Sorrentino R, Fazio V, Canonico ME, Chiariello L, *et al.* Prominent basal and middle strain longitudinal involvement in newly-diagnosed and never treated hypertensive patients without clear-cut hypertrophy. *Int J Cardiol* 2020; 304:179–184.
22. Rudolph A, Abdel-Aty H, Bohl S, Boyé P, Zagrosek A, Dietz R, *et al.* Noninvasive detection of fibrosis applying contrast-enhanced cardiac magnetic resonance in different forms of left ventricular hypertrophy relation to remodeling. *J Am Coll Cardiol* 2009; 53:284–291.
23. Kouzu H, Yuda S, Muranaka A, Doi T, Yamamoto H, Shimoshige S, *et al.* Left ventricular hypertrophy causes different changes in longitudinal, radial, and circumferential mechanics in patients with hypertension: a two-dimensional speckle tracking study. *J Am Soc Echocardiogr* 2011; 24:192–199.
24. Gnakamene JB, Safar ME, Levy BI, Escoubet B. Left ventricular torsion associated with aortic stiffness in hypertension. *J Am Heart Assoc* 2018; 7:e007427.
25. Tadic M, Cuspidi C, Vukomanovic V, Ilic S, Obert P, Kocijancic V, *et al.* Layer-specific deformation of the left ventricle in uncomplicated patients with type 2 diabetes and arterial hypertension. *Arch Cardiovasc Dis* 2018; 111:17–24.
26. Kim D, Shim CY, Hong GR, Park S, Cho I, Chang HJ, *et al.* Differences in left ventricular functional adaptation to arterial stiffness and neurohormonal activation in patients with hypertension: a study with two-dimensional layer-specific speckle tracking echocardiography. *Clin Hypertens* 2017; 23:21.
27. Tadic M, Cuspidi C, Vukomanovic V, Celic V, Tasic I, Stevanovic A, Kocijancic V. Does masked hypertension impact left ventricular deformation? *J Am Soc Hypertens* 2016; 10:694–701.
28. Lee WH, Liu YW, Yang LT, Tsai WC. Prognostic value of longitudinal strain of subepicardial myocardium in patients with hypertension. *J Hypertens* 2016; 34:1195–1200.
29. Lembo M, Santoro C, Sorrentino R, Canonico ME, Fazio V, Trimarco B, *et al.* Interrelation between midwall mechanics and longitudinal strain in newly diagnosed and never-treated hypertensive patients without clinically defined hypertrophy. *J Hypertens* 2020; 38:295–302.
30. Manganaro R, Marchetta S, Dulgheru R, Sugimoto T, Tsugu T, Ilardi F, *et al.* Correlation between noninvasive myocardial work indices and main parameters of systolic and diastolic function: results from the EACVI NORRE study. *Eur Heart JCardiovasc Imaging* 2020; 21:533–541.
31. Tadic M, Cuspidi C, Pencic B, Grassi G, Celic V. Myocardial work in hypertensive patients with and without diabetes: an echocardiographic study. *J Clin Hypertens (Greenwich)* 2020; 22:2121–2127.
32. Chan J, Edwards NFA, Khandheria BK, Shiino K, Sabapathy S, Anderson B, *et al.* A new approach to assess myocardial work by noninvasive left ventricular pressure-strain relations in hypertension and dilated cardiomyopathy. *Eur Heart J Cardiovasc Imaging* 2019; 20:31–39.
33. El Mahdiui M, van der Bijl P, Abou R, Ajmone Marsan N, Delgado V, Bax JJ. Global left ventricular myocardial work efficiency in healthy individuals and patients with cardiovascular disease. *J Am Soc Echocardiogr* 2019; 32:1120–1127.
34. Tadic M, Cuspidi C, Pencic B, Vukomanovic V, Taddei S, Grassi G, Celic V. Association between myocardial work and functional capacity in patients with arterial hypertension: an echocardiographic study. *Blood Press* 2021; 30:188–195.
35. Loncaric F, Marciniak M, Nunno L, Mimbrero M, Fernandes JF, Fabijanovic D, *et al.* Distribution of myocardial work in arterial hypertension: insights from noninvasive left ventricular pressurestrain relations. *Int J Cardiovasc Imaging* 2021; 37:145–154.
36. Saito M, Khan F, Stoklosa T, Iannaccone A, Negishi K, Marwick TH. Prognostic implications of LV strain risk score in asymptomatic patients with hypertensive heart disease. *JACC Cardiovasc Imaging* 2016; 9:911–921.
37. Galderisi M, Cosyns B, Edvardsen T, Cardim N, Delgado V, Di Salvo G, *et al.* Standardization of adult transthoracic echocardiography reporting in agreement with recent chamber quantification, diastolic function, and heart valve disease recommendations: an expert consensus document of the European Association of Cardiovascular Imaging. *Eur Heart J Cardiovasc Imaging* 2017; 18:1301–1310.
38. Oketona OA, Balogun MO, Akintomide AO, Ajayi OE, Adebayo RA, Mene-Afejuku TO, *et al.* Right ventricular systolic function in hypertensive heart failure. *Vasc Health Risk Manag* 2017; 13:353–360.
39. Pedrinelli R, Canale ML, Giannini C, Talini E, Penno G, Dell'Omo G, *et al.* Right ventricular dysfunction in early systemic hypertension: a tissue Doppler imaging study in patients with high-normal and mildly increased arterial blood pressure. *J Hypertens* 2010; 28:615–621.
40. Tadic M, Cuspidi C, Vukomanovic V, Ilic S, Celic V, Obert P, *et al.* The influence of type 2 diabetes and arterial hypertension on right ventricular layer-specific mechanics. *Acta Diabetol* 2016; 53:791–797.
41. Tadic M, Cuspidi C, Suzic-Lazic J, Andric A, Stojcevski B, Ivanovic B, *et al.* Is there a relationship between right-ventricular and right atrial mechanics and functional capacity in hypertensive patients? *J Hypertens* 2014; 32:929–937.
42. Mondillo S, Cameli M, Caputo ML, Lisi M, Palmerini E, Padeletti M, *et al.* Early detection of left atrial strain abnormalities by speckle-tracking in hypertensive and diabetic patients with normal left atrial size. *J Am Soc Echocardiogr* 2011; 24:898–908.
43. Chen XJ, Chen C, Liang YJ, Gao XL, Jiang J, Kang Y, *et al.* Decreased left atrial myocardial strain in patients with suboptimal blood pressure control. *Clin Exp Hypertens* 2017; 39:481–488.
44. Cameli M, Mandoli GE, Lisi E, Ibrahim A, Incampo E, Buccoliero G, *et al.* Left atrial, ventricular and atrio-ventricular strain in patients with subclinical heart dysfunction. *Int J Cardiovasc Imaging* 2019; 35:249–258.
45. Braunauer K, Düngen HD, Belyavskiy E, Aravind-Kumar R, Frydas A, Kropf M, *et al.* Potential usefulness and clinical relevance of a novel left atrial filling index to estimate left ventricular filling pressures in patients with preserved left ventricular ejection fraction. *Eur Heart J Cardiovasc Imaging* 2020; 21:260–269.
46. de Simone G, Mancusi C, Esposito R, De Luca N, Galderisi M. Echocardiography in arterial hypertension. *High Blood Press Cardiovasc Prev* 2018; 25:159–166.
47. Jarasunas J, Aidietis A, Aidietiene S. Left atrial strain: an early marker of left ventricular diastolic dysfunction in patients with hypertension and paroxysmal atrial fibrillation. *Cardiovasc Ultrasound* 2018; 16:29.
48. Teixeira R, Vieira MJ, Gonçalves A, Cardim N, Gonçalves L. Ultrasonographic vascular mechanics to assess arterial stiffness: a review. *Eur Heart J Cardiovasc Imaging* 2016; 17:233–246.
49. Catalano M, Lamberti-Castronuovo A, Catalano A, Filocamo D, Zimbalatti C. Two-dimensional speckle-tracking strain imaging in the assessment of mechanical properties of carotid arteries: feasibility and comparison with conventional markers of subclinical atherosclerosis. *Eur J Echocardiogr* 2011; 12:528–535.
50. Pouleur AC, le Polain de Waroux JB, Pasquet A, Gerber BL, Gérard O, Allain P, *et al.* Assessment of left ventricular mass and volumes by three-dimensional echocardiography in patients with or without wall motion abnormalities: comparison against cine magnetic resonance imaging. *Heart* 2008; 94:1050–1057.
51. Yap SC, van Geuns RJ, Nemes A, Meijboom FJ, McGhie JS, Geleijnse ML, *et al.* Rapid and accurate measurement of LV mass by biplane realtime 3D echocardiography in patients with concentric LV hypertrophy: comparison to CMR. *Eur J Echocardiogr* 2008; 9:255–260.
52. Mor-Avi V, Sugeng L, Weinert L, MacEneaney P, Caiani EG, Koch R, *et al.* Fast measurement of left ventricular mass with real-time three-dimensional echocardiography: comparison with magnetic resonance imaging. *Circulation* 2004; 110:1814–1818.
53. Marwick TH, Gillebert TC, Aurigemma G, Chirinos J, Derumeaux G, Galderisi M, *et al.* Recommendations on the use of echocardiography in adult hypertension: a report from the European Association of Cardiovascular Imaging (EACVI) and the American Society of Echocardiography (ASE). *Eur Heart J Cardiovasc Imaging* 2015; 16:577–605.
54. Lembo M, Esposito R, Santoro C, Lo Iudice F, Schiano-Lomoriello V, Fazio V, *et al.* Three-dimensional echocardiographic ventricular mass/end-diastolic volume ratio in native hypertensive patients: relation between stroke volume and geometry. *J Hypertens* 2018; 36:1697–1704.

55. Heckbert SR, Post W, Pearson GD, Arnett DK, Gomes AS, Jerosch-Herold M, *et al.* Traditional cardiovascular risk factors in relation to left ventricular mass, volume, and systolic function by cardiac magnetic resonance imaging: the Multiethnic Study of Atherosclerosis. *J Am Coll Cardiol* 2006; 48:2285–2292.
56. Petitto M, Esposito R, Sorrentino R, Lembo M, Luciano F, De Roberto AM, *et al.* Sex-specific echocardiographic reference values: the women's point of view. *J Cardiovasc Med (Hagerstown)* 2018; 19:527–535.
57. Galderisi M, Esposito R, Schiano-Lomoriello V, Santoro A, Ippolito R, Schiattarella P, *et al.* Correlates of global area strain in native hypertensive patients: a three-dimensional speckle-tracking echocardiography study. *Eur Heart J Cardiovasc Imaging* 2012; 13:730–738.
58. Navarini S, Bellsham-Revell H, Chubb H, Gu H, Sinha MD, Simpson JM. Myocardial deformation measured by 3-dimensional speckle tracking in children and adolescents with systemic arterial hypertension. *Hypertension* 2017; 70:1142–1147.
59. Saltijeral A, Perez de Isla L, Veras K, Fernandez Mde J, Gorissen W, Rementeria J, *et al.* Myocardial strain characterization in different left ventricular adaptative responses to high blood pressure: a study based on 3D-wall motion tracking analysis. *Echocardiography* 2010; 27:1238–1246.
60. Santoro C, Arpino G, Esposito R, Lembo M, Paciolla I, Cardalesi C, *et al.* 2D and 3D strain for detection of subclinical anthracycline cardiotoxicity in breast cancer patients: a balance with feasibility. *Eur Heart J Cardiovasc Imaging* 2017; 18:930–936.
61. Tadic M, Cuspidi C, Vukomanovic V, Kocijancic V, Celic V. Right ventricular remodeling and updated left ventricular geometry classification: is there any relationship? *Blood Press* 2016; 25:292–297.
62. Kanar B, Ozben B, Kanar HS, Arsan A, Tigen K. Left atrial volume changes are an early marker of end-organ damage in essential hypertension: a multidisciplinary approach to an old problem. *Echocardiography* 2017; 34:1895–1902.
63. Esposito G, Piras P, Evangelista A, Nuzzi V, Nardinocchi P, Pannarale G, *et al.* Improving performance of 3D speckle tracking in arterial hypertension and paroxysmal atrial fibrillation by using novel strain parameters. *Sci Rep* 2019; 9:7382.
64. Vasconcellos HD, Moreira HT, Ciuffo L, Nwabuo CC, Yared GS, Ambale-Venkatesh B, *et al.* Cumulative blood pressure from early adulthood to middle age is associated with left atrial remodelling and subclinical dysfunction assessed by three-dimensional echocardiography: a prospective post hoc analysis from the coronary artery risk development in young adults study. *Eur Heart J Cardiovasc Imaging* 2018; 19:977–984.
65. Maceira AM, Prasad SK, Khan M, Pennell DJ. Normalized left ventricular systolic and diastolic function by steady state free precession cardiovascular magnetic resonance. *J Cardiovasc Magn Reson* 2006; 8:417–426.
66. Khouri MG, Peshock RM, Ayers CR, de Lemos JA, Drazner MH. A 4-tiered classification of left ventricular hypertrophy based on left ventricular geometry: the Dallas heart study. *Circ Cardiovasc Imaging* 2010; 3:164–171.
67. Garg S, de Lemos JA, Ayers C, Khouri MG, Pandey A, Berry JD, *et al.* Association of a 4-tiered classification of LV hypertrophy with adverse CV outcomes in the general population. *JACC Cardiovasc Imaging* 2015; 8:1034–1041.
68. Puntmann VO, Jahnke C, Gebker R, Schnackenburg B, Fox KF, Fleck E, *et al.* Usefulness of magnetic resonance imaging to distinguish hypertensive and hypertrophic cardiomyopathy. *Am J Cardiol* 2010; 106:1016–1022.
69. Vogelsberg H, Mahrholdt H, Deluigi CC, Yilmaz Z, Kispert EM, Greulich S, *et al.* Cardiovascular magnetic resonance in clinically suspected cardiac amyloidosis: noninvasive imaging compared to endomyocardial biopsy. *J Am Coll Cardiol* 2008; 51:1022–1030.
70. Moreo A, Ambrosio G, De Chiara B, Pu M, Tran T, Mauri F, *et al.* Influence of myocardial fibrosis on left ventricular diastolic function: noninvasive assessment by cardiac magnetic resonance and echo. *Circ Cardiovasc Imaging* 2009; 2:437–443.
71. Moon JC, Messroghli DR, Kellman P, Piechnik SK, Robson MD, Ugander M, *et al.* Myocardial T1 mapping and extracellular volume quantification: a Society for Cardiovascular Magnetic Resonance (SCMR) and CMR Working Group of the European Society of Cardiology consensus statement. *J Cardiovasc Magn Reson* 2013; 15:92.
72. Scully PR, Bastarrika G, Moon JC, Treibel TA. Myocardial extracellular volume quantification by Cardiovascular Magnetic resonance and computed tomography. *Curr Cardiol Rep* 2018; 20:15.
73. Kuruvilla S, Janardhanan R, Antkowiak P, Keeley EC, Adenaw N, Brooks J, *et al.* Increased extracellular volume and altered mechanics are associated with LVH in hypertensive heart disease, not hypertension alone. *JACC Cardiovasc Imaging* 2015; 8:172–180.
74. Treibel TA, Zemrak F, Sado DM, Banypersad SM, White SK, Maestrini V, *et al.* Extracellular volume quantification in isolated hypertension: changes at the detectable limits? *J Cardiovasc Magn Reson* 2015; 17:74.
75. Pan JA, Michaëlsson E, Shaw PW, Kuruvilla S, Kramer CM, Gan LM, *et al.* Extracellular volume by cardiac magnetic resonance is associated with biomarkers of inflammation in hypertensive heart disease. *J Hypertens* 2019; 37:65–72.
76. Bernhardt P, Levenson B, Albrecht A, Engels T, Strohm O. Detection of cardiac small vessel disease by adenosine-stress magnetic resonance. *Int J Cardiol* 2007; 121:261–266.
77. Kim RJ, Fieno DS, Parrish TB, Harris K, Chen EL, Simonetti O, *et al.* Relationship of MRI delayed contrast enhancement to irreversible injury, infarct age, and contractile function. *Circulation* 1999; 100: 1992–2002.
78. Todiere G, Neglia D, Ghione S, Fommei E, Capozza P, Guarini G, *et al.* Right ventricular remodelling in systemic hypertension: a cardiac MRI study. *Heart* 2011; 97:1257–1261.
79. van Hout MJ, Scholte AJ, Juffermans JF, Westenberg JJ, Zhong L, Zhou X, *et al.* How to measure the aorta using MRI: a practical guide. *J Magn Reson Imaging* 2020; 52:971–977.
80. Porcu M, Mannelli L, Melis M, Suri JS, Gerosa C, Cerrone G, *et al.* Carotid plaque imaging profiling in subjects with risk factors (diabetes and hypertension). *Cardiovasc Diagn Ther* 2020; 10:1005–1018.
81. Takaya N, Yuan C, Chu B, Saam T, Underhill H, Cai J, *et al.* Association between carotid plaque characteristics and subsequent ischemic cerebrovascular events: a prospective assessment with MRI–initial results. *Stroke* 2006; 37:818–823.
82. Pedrizzetti G, Claus P, Kilner PJ, Nagel E. Principles of cardiovascular magnetic resonance feature tracking and echocardiographic speckle tracking for informed clinical use. *J Cardiovasc Magn Reson* 2016; 18:51.
83. Scatteia A, Baritussio A, Bucciarelli-Ducci C. Strain imaging using cardiac magnetic resonance. *Heart Fail Rev* 2017; 22:465–476.
84. Liu H, Wang J, Pan Y, Ge Y, Guo Z, Zhao S. Early and quantitative assessment of myocardial deformation in essential hypertension patients by using cardiovascular magnetic resonance feature tracking. *Sci Rep* 2020; 10:3582.
85. Niu J, Zeng M, Wang Y, Liu J, Li H, Wang S, *et al.* Sensitive marker for evaluation of hypertensive heart disease: extracellular volume and myocardial strain. *BMC Cardiovasc Disord* 2020; 20:292.
86. Zhang Z, Ma Q, Cao L, Zhao Z, Zhao J, Lu Q, et al. *Correlation between left ventricular myocardial strain and left ventricular geometry in healthy adults: a cardiovascular magnetic resonance-feature tracking study.*
87. Li L, Chen X, Yin G, Yan W, Cui C, Cheng H, *et al.* Early detection of left atrial dysfunction assessed by CMR feature tracking in hypertensive patients. *Eur Radiol* 2020; 30:702–711.
88. Paelinck BP, de Roos A, Bax JJ, Bosmans JM, van Der Geest RJ, Dhondt D, *et al.* Feasibility of tissue magnetic resonance imaging: a pilot study in comparison with tissue Doppler imaging and invasive measurement. *J Am Coll Cardiol* 2005; 45:1109–1116.
89. Westenberg JJ, Roes SD, Ajmone Marsan N, Binnendijk NM, Doornbos J, Bax JJ, *et al.* Mitral valve and tricuspid valve blood flow: accurate quantification with 3D velocity-encoded MR imaging with retrospective valve tracking. *Radiology* 2008; 249:792–800.
90. Kühl JT, Nielsen JB, Stisen ZR, Fuchs A, Sigvardsen PE, Graff C, *et al.* Left ventricular hypertrophy identified by cardiac computed tomography and ECG in hypertensive individuals: a population-based study. *J Hypertens* 2019; 37:739–746.
91. Boogers MJ, van Werkhoven JM, Schuijf JD, Delgado V, El-Naggar HM, Boersma E, *et al.* Feasibility of diastolic function assessment with cardiac CT: feasibility study in comparison with tissue Doppler imaging. *JACC Cardiovasc Imaging* 2011; 4:246–256.
92. Nacif MS, Kawel N, Lee JJ, Chen X, Yao J, Zavodni A, *et al.* nterstitial myocardial fibrosis assessed as extracellular volume fraction with low-radiation-dose cardiac CT. *Radiology* 2012; 264:876–883.

93. Kumar V, Harfi TT, He X, McCarthy B, Cardona A, Simonetti OP, *et al*. Estimation of myocardial fibrosis in humans with dual energy CT. *J Cardiovasc Comput Tomogr* 2019; 13:315–318.
94. Cuspidi C, Meani S, Negri F, Sala C, Mancia G. Left ventricular hypertrophy and abdominal aorta size in essential hypertension. *J Hypertens* 2011; 29:1213–1219.
95. Brown LC, Powell JT. Risk factors for aneurysm rupture in patients kept under ultrasound surveillance: UK Small Aneurysm Trial participants. *Ann Surg* 1999; 230:289–296.
96. Hirsch AT, Haskal ZJ, Hertzer NR, Bakal CW, Creager MA, Halperin JL, *et al*. ACC/AHA 2005 Practice Guidelines for the management of patients with peripheral arterial disease. *Circulation* 2006; 113:e463–e654.
97. Schwartz SI, Durham C, Clouse WD, Patel VI, Lancaster RT, Cambria RP, *et al*. Predictors of late aortic intervention in patients with medically treated type B aortic dissection. *J Vasc Surg* 2018; 67:78–84.
98. Nakanishi R, Baskaran L, Gransar H, Budoff MJ, Achenbach S, Al-Mallah M, *et al*. Relationship of hypertension to coronary atherosclerosis and cardiac events in patients with coronary computed tomographic angiography. *Hypertension* 2017; 70:293–299.
99. Benson JC, Lanzino G, Nardi V, Savastano L, Lerman A, Brinjikji W. Semiautomated carotid artery plaque composition: are intraplaque CT imaging features associated with cardiovascular risk factors? *Neuroradiology* 2021; doi:10.1007/s00234-021-02662-6 [Epub ahead of print].
100. Rieck AE, Cramariuc D, Boman K, Gohlke-Bärwolf C, Staal EM, Lønnebakken MT, *et al*. Hypertension in aortic stenosis: implications for left ventricular structure and cardiovascular events. *Hypertension* 2012; 60:90–97.
101. Cartlidge TR, Bing R, Kwiecinski J, Guzzetti E, Pawade TA, Doris MK, *et al*. Contrast-enhanced computed tomography assessment of aortic stenosis. *Heart* 2021; heartjnl-2020-318556. doi: 10.1136/heartjnl-2020-318556.[Epub ahead of print].
102. Baumgartner H, Hung J, Bermejo J, Chambers JB, Edvardsen T, Goldstein S, *et al*. Recommendations on the echocardiographic assessment of aortic valve stenosis: a focused update from the European Association of Cardiovascular Imaging and the American Society of Echocardiography. *J Am Soc Echocardiogr* 2017; 30:372–392.
103. Pibarot P, Dumesnil JG. Paradoxical low-flow, low-gradient aortic stenosis: new evidence, more questions. *Circulation* 2013; 128:1729–1732.
104. Gallamini A, Zwarthoed C, Borra A. Positron emission tomography (PET) in oncology. *Cancers* 2014; 6:1821–1889.
105. Seraj SM, Pournazari K, Ayubcha C, Jahangiri P, Khosravi M, Werner T, *et al*. Global assessment of joints in patients with rheumatoid arthritis: quantification of inflammatory lesions in FDG-PET. *J Nucl Med* 2018; 59 (Suppl 1):1208.
106. Shivamurthy VK, Tahari AK, Marcus C, Subramaniam RM. Brain FDG PET and the diagnosis of dementia. *Am J Roentgenol* 2015; 204:W76–W85.
107. Rojulpote C, Mehdizadeh Seraj S, Zirakchian Zadeh M, Yadav D, Raynor WY, Kothekar E, Al-Zaghal A, *et al*. Role of FDG-PET/CT in assessing the correlation between blood pressure and myocardial metabolic uptake. *Asia Ocean J Nucl Med Biol* 2020; 8:36–45.
108. Alexander RW. Hypertension and the pathogenesis of atherosclerosis. Oxidative stress and the mediation of arterial inflammatory response: a new perspective. *Hypertension* 1995; 25:155–161.
109. Rudd JH, Warburton EA, Fryer TD, Jones HA, Clark JC, Antoun N, *et al*. Imaging atherosclerotic plaque inflammation with [18F]-fluorodeoxyglucose positron emission tomography. *Circulation* 2002; 105:2708–2711.
110. Tawakol A, Migrino RQ, Bashian GG, Bedri S, Vermylen D, Cury RC, *et al*. In vivo 18F-fluorodeoxyglucose positron emission tomography imaging provides a noninvasive measure of carotid plaque inflammation in patients. *J Am Coll Cardiol* 2006; 48:1818–1824.
111. Marnane M, Merwick A, Sheehan OC, Hannon N, Foran P, Grant T, *et al*. Carotid plaque inflammation on 18F-fluorodeoxyglucose positron emission tomography predicts early stroke recurrence. *Ann Neurol* 2012; 71:709–718.
112. Creager MD, Hohl T, Hutcheson JD, Moss AJ, Schlotter F, Blaser MC, Park MA, *et al*. 18F-fluoride signal amplification identifies microcalcifications associated with atherosclerotic plaque instability in positron emission tomography/computed tomography images. *Circ Cardiovasc Imaging* 2019; 12:e007835.
113. Fletcher AJ, Lembo M, Kwiecinski J, Syed MBJ, Nash J, Tzolos E, *et al*. Quantifying microcalcification activity in the thoracic aorta. *J Nucl Cardiol* 2021; doi:10.1007/s12350-020-02458-w [Epub ahead of print].
114. Rojulpote C, Patil S, Gonuguntla K, Karambelkar P, Bravo PE, Seraj SM, *et al*. NaF-PET/CT global assessment in detecting and quantifying subclinical cardiac atherosclerosis and its association with blood pressure in nondyslipidemic individuals. *Am J Cardiovasc Dis* 2020; 10:101–107.
115. Fujimoto K, Norikane T, Yamamoto Y, Takami Y, Mitamura K, Okada M, *et al*. Association between carotid 18F-NaF and 18F-FDG uptake on PET/CT with ischemic vascular brain disease on MRI in patients with carotid artery disease. *Ann Nucl Med* 2019; 33:907–915.
116. Dweck MR, Jones C, Joshi NV, Fletcher AM, Richardson H, White A, *et al*. Assessment of valvular calcification and inflammation by positron emission tomography in patients with aortic stenosis. *Circulation* 2012; 125:76–86.
117. Gaudieri V, Mannarino T, Zampella E, Assante R, D'Antonio A, Nappi C, *et al*. Prognostic value of coronary vascular dysfunction assessed by rubidium-82 PET/CT imaging in patients with resistant hypertension without overt coronary artery disease. *Eur J Nucl Med Mol Imaging* 2021; doi:10.1007/s00259-021-05239-w. [Epub ahead of print].